Design of a thin-plate based tunable high-quality narrow passband filter for elastic transverse waves propagate in metals

J. Zhang, L. H. Zeng, C. L. Hu, W. S. Yan, Yan Pennec, and N. Hu

Citation: AIP Advances **8**, 035323 (2018); doi: 10.1063/1.5023517
View online: https://doi.org/10.1063/1.5023517
View Table of Contents: http://aip.scitation.org/toc/adv/8/3
Published by the American Institute of Physics

Design of a thin-plate based tunable high-quality narrow passband filter for elastic transverse waves propagate in metals

J. Zhang,[1,a] L. H. Zeng,[1] C. L. Hu,[2] W. S. Yan,[3] Yan Pennec,[4] and N. Hu[1,5,b]
[1]*College of Aerospace Engineering, Chongqing University, Chongqing 400044, P. R. China*
[2]*State Key Laboratory of Silicate Materials for Architecture, Wuhan University of Technology, Wuhan 430070, P. R. China*
[3]*Institute of Microstructure Technology (IMT), Karlsruhe Institute of Technology, Hermann-von-Helmholtz-Platz 1, 76344 Eggenstein-Leopoldshafen, Germany*
[4]*Institut d'Electronique, de Microélectronique et de Nanotechnologie (IEMN-UMR CNRS 8520), Université de Lille, Villeneuve d'Ascq, France*
[5]*Key Laboratory of Optoelectronic Technology and Systems of the Education Ministry of China, Chongqing University, Chongqing 400044, China*

(Received 25 January 2018; accepted 20 March 2018; published online 29 March 2018)

For the elastic SV (transverse) waves in metals, a high-quality narrow passband filter that consists of aligned parallel thin plates with small gaps is designed. In order to obtain a good performance, the thin plates should be constituted by materials with a smaller mass density and Young's modulus, such as polymethylmethacrylate (PMMA), compared to the embedded materials in which the elastic SV waves propagate. Both the theoretical model and the full numerical simulation show that the transmission spectrum of the designed filter demonstrates several peaks with flawless transmission within 0 KHz ~20 KHz frequency range. The peaks can be readily tuned by manipulating the geometrical parameters of the plates. Therefore, the current design works well for both low and high frequencies with a controllable size. Even for low frequencies on the order of kilohertz, the size of this filter can be still limited to the order of centimeters, which significantly benefits the real applications. The investigation also finds that the same filter is valid when using different metals and the reason behind this is explained theoretically. Additionally, the effect of bonding conditions of interfaces between thin plates and the base material is investigated using a spring model. https://doi.org/10.1063/1.5023517

I. INTRODUCTION

During the past decade, design of filters/isolators for classical waves has attracted great attentions due to their wide employment in various applications such as wave signal processing system and noise/vibration controlling. The existence of forbidden band gaps allows phononic crystals (PnCs) to become a potential candidate for the design of filters/isolators for acoustic and elastic waves.[1–3] Controlled by the Bragg scattering mechanism, the forbidden bandwidth of PnCs is typically narrow and the waves inside the band gaps are of the wavelength at the same order as the lattice constants of PnCs. As a result, the PnCs-based design usually serves as a broad passband filter and an unmanageable size is needed for low frequency problems. This has consequently led to the increased research effort to increase the forbidden bandwidth[4–7] and to decrease the working frequency of PnCs. The pioneer

[a]E-mail: mejzhang@cqu.edu.cn;
[b]ninghu@cqu.edu.cn

work of Liu et al.[8] by incorporating local resonators[9] into PnCs, which are usually referred to as metamaterials, provided a very efficient way to reduce the working frequency of PnCs. Compared with PnCs, the working frequency of these metamaterials is significantly reduced by one or more orders of magnitude. It is in this spirit that, during the past several years, various acoustic and elastic metamaterials were designed mainly in the forms of 1D mass-spring model,[10–14] beams,[15–21] plates with single[22–26] and double[26–30] sided stubs, membranes,[31–36] as well as 2D metamaterials.[2,37–40] To make the metamaterials more adaptive, more recently, several tunable local resonators were designed.[41–49]

To date, although the above introduced various PnCs and metamaterials have been proposed, it should be noted that they typically work well as broad passband ones. However, the design of filters with a narrow passband is still not sufficient. Khelif et al.[2,50] proposed a narrow passband acoustic 2D PnC based filter composed of a square array of hollow steel cylinders embedded in water. The frequency at which the narrow passband occurs can be tuned by the inner radius of hollow steel cylinders. Inspired by the structure of biomaterials, a multilayered model with a hierarchical structure was proposed by Zhang,[51] the reflection spectrum indicates that such multilayered model works efficiently as a narrow passband filter for P- and SV- waves of ultra-high frequencies. Besides, a narrow passband filter was realized through the impedance-mirroring by Lee and Kim.[52,53] Additionally, there exists a technique of inserting a cavity/defect inside the waveguide parts made of PnCs to yield a narrow passband.[37,54] In brief, the above various narrow passband filters still inherit the characteristic of PnCs, that the narrow passband occurs at relatively high frequencies i.e., few megahertz in millimeter size structures. A narrow passband filter working at relatively low frequencies is still less considered.[55,56]

As the basic mechanical element, the dynamic behavior of thin plates has been well investigated. Therefore, as mentioned before, various thin plates based PnCs and metamaterials have been proposed. In our previous work,[57] we designed a thin plate based narrow passband filter for elastic SV waves propagating in metal blocks. The filter is composed of aligned parallel thin PMMA plates, which are separated by small gaps, and are seamlessly bonded at the two ends to the base blocks. Both theoretical model and numerical simulations show that the transmission spectrum of this filter has several sharp peaks with flawless transmission. The peaks at which the narrow passband occurs can be tuned by the length of plates. Therefore, the designed filter is effective for both low and high frequencies. Even for low frequencies on the order of kilohertz, the size (length of the plates) of this filter can be still confined to the order of centimeters. Moreover, the peaks occur at the same frequency points for different base materials.

However, in our previous paper, it is found that the theoretical solutions in which the plate is modelled by the Kirchhoff plate theory agree well with numerical simulations at low frequencies, while deviating from them at relatively high frequencies. Moreover, only the PMMA is considered for the plates and the physical mechanism behind the fact that the base material does not change the peaks is not well understood and clarified. Additionally, in our previous work, the interfaces between plates and the base matrix is assumed to be perfect, other situations have not been considered.

In the current work, we attempt to provide a more comprehensive study on the above listed problems, which is important to well understand the design. Specifically, the Mindlin plate theory taking the rotatory inertia and shear deformation effects into account is adopted to describe the thin plates.[58] The corresponding theoretical model is solved using two different techniques: one is a semi-analytical method and the other is a full analytical method. The results show that solutions based upon the Mindlin plate theory agree better with numerical simulations than the Kirchhoff plate theory. Results indicate that the peaks occur at the natural frequencies of the plate with fixed displacement or opposite displacements at two ends. Besides the PMMA, other potential materials being suitable to fabricate the thin plates are explored and the bonding conditions between the thin plates and the base material on the performance of this filter are investigated through a spring model.

The outline of the paper is described as follows. In Section II, the design of this filter is introduced briefly. Then, in Section III, two theoretical models are proposed and solved to evaluate the transmission spectrum of this filter using two different techniques, in particular, the one to divide the conventional transmission into a symmetric and anti-symmetric modes. The Finite Element Method

(FEM) numerical model used to evaluate the performance of this filter is introduced in Section IV. The results are presented in Section V and followed by a short conclusion in Section VI.

II. DESIGN OF THE FILTER

Figure 1 demonstrates a schematic of this filter, where the thickness and length of the plates are denoted by h and L, and the gap between adjacent plates is denoted by a. Here, a is much smaller than h. The propagation of SV waves is along the horizontal direction and the material particles vibrate along the vertical direction as indicated by the short arrows. The thin plates are made up of a single material, such as PMMA used in our previous paper, other potential materials being suitable to make the plates are mentioned later.

III. THEORETICAL MODEL FOR THE TRANSMISSION SPECTRUM OF THIS FILTER

In this work, Young's modulus, shear modulus, Poisson's ratio, and mass density are denoted by E, μ, υ, and ρ, respectively. In the Kirchhoff plate theory, the governing equation for flexural waves under a harmonic loading is expressed as:[59]

$$D\frac{\partial^4 w}{\partial x^4} - \rho h\omega^2 w = 0 \tag{1}$$

Here,ω is the angular frequency, w is the flexural displacement, and $D = Eh^3/12(1-\upsilon^2)$ is the bending stiffness of the plate. Expressing the general solution for Eq. (1) in the form of $w(x) = e^{kx}$ and substituting it into Eq. (1) yields $k^4 = \rho h\omega^2/D$. Therefore, four solutions for k are $k_{1,2} = \pm\mathbf{i}\sqrt[4]{\rho h\omega^2/D}$ and $k_{3,4} = \pm\sqrt[4]{\rho h\omega^2/D}$, where $\mathbf{i}$ denotes the imaginary part. In our previous paper and the work by Su and Norris,[60] it is found that the theoretical solutions based on the Kirchhoff plate theory deviate from the numerical simulations, in particular at high frequencies. The reasons behind this mainly include that the rotatory inertia and shear deformation effects are neglected in the Kirchhoff theory. Hence, in the current work, in order to obtain more accurate results, the Mindlin plate theory is employed. The same treatment has also been considered in the recent work by Su etc.[58] The corresponding governing equation becomes:

$$D\frac{\partial^4 w}{\partial x^4} + \omega^2\left(\frac{\rho h^3}{12} + \frac{\rho D}{\chi\mu}\right)\frac{\partial^2 w}{\partial x^2} + \left(\frac{\rho^2 h^3}{12\chi\mu}\omega^4 - \rho h\omega^2\right)w = 0 \tag{2}$$

where χ is the Timoshenko shear coefficient, which is normally set to be 5/6 for a rectangular section. Similarly, general solution to Eq. (2) can be expressed in the form $w(x) = e^{kx}$ as before. Four values

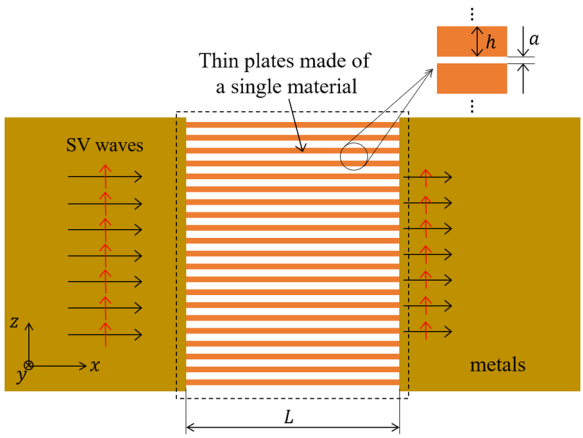

FIG. 1. 2D Schematic of the filter made by aligned parallel thin plates for elastic SV waves propagating in metals.

for k under the Mindlin plate theory can be solved as:

$$k_{1,2} = \pm \mathbf{i}\sqrt{\frac{\beta^2}{2} + \sqrt{\left(\frac{\beta^2}{2}\right)^2 + \gamma^4}}$$
$$k_{3,4} = \pm \sqrt{-\frac{\beta^2}{2} + \sqrt{\left(\frac{\beta^2}{2}\right)^2 + \gamma^4}} \tag{3}$$

with $\beta^2 = \left(\frac{\rho h^3}{12D} + \frac{\rho}{\chi\mu}\right)\omega^2$ and $\gamma^4 = \left(\frac{\rho h}{D}\omega^2 - \frac{\rho^2 h^3}{12\chi\mu D}\omega^4\right)$. Different from those in the Kirchhoff theory, the magnitude of $k_{1,2}$ is different from that of $k_{3,4}$ in the Mindlin plate theory. In order to obtain the transmission spectrum of this filter, a unit cell as proposed in Ref. 60 is adopted as shown in FIG. 2. Under a normal incidence of a plane elastic SV wave, the wave fields in the unit cell can be expressed as:

$$w(x) = \begin{cases} e^{\mathbf{i}k_T x} + Re^{-\mathbf{i}k_T x}, x < -\dfrac{L}{2} \\ Ae^{k_1 x} + Be^{k_2 x} + Ue^{k_3 x} + Ve^{k_4 x}, |x| < \dfrac{L}{2} \\ Te^{\mathbf{i}k_T x}, x > \dfrac{L}{2} \end{cases} \tag{4}$$

The parameters R, A, B, U, V, and T are the coefficients of displacements for the reflected wave, the forward and backward waves in the plate, and the transmitted wave. $k_T = \omega/c_T$ is the wave number of transverse waves in the base material, in which the corresponding wave speed is $c_T = \sqrt{E/2\rho(1+\upsilon)}$.

The six unknowns (R, A, B, U, V, and T) are determined by the z-averaged continuity conditions of displacement, rotation angle, and shear force at $x = -L/2$ and $x = L/2$ as follows:[60]

$$\begin{cases} z_0^{-\mathbf{i}} + Rz_0^{\mathbf{i}} = Az_1^{-1} + Bz_2^{-1} + Uz_3^{-1} + Vz_4^{-1} \\ z_0^{-\mathbf{i}} - Rz_0^{\mathbf{i}} = \dfrac{1}{\mathbf{i}k_T}\left(Ak_1 z_1^{-1} + Bk_2 z_2^{-1} + Uk_3 z_3^{-1} + Vk_4 z_4^{-1}\right) \\ z_0^{-\mathbf{i}} - Rz_0^{\mathbf{i}} = \dfrac{D\mathbf{i}}{\mu^{(0)} h' k_T}\left(Ak_1^3 z_1^{-1} + Bk_2^3 z_2^{-1} + Uk_3^3 z_3^{-1} + Vk_4^3 z_4^{-1}\right) \\ Tz_0^{\mathbf{i}} = Az_1 + Bz_2 + Uz_3 + Vz_4 \\ Tz_0^{\mathbf{i}} = \dfrac{1}{\mathbf{i}k_T}\left(Ak_1 z_1 + Bk_2 z_2 + Uk_3 z_3 + Vk_4 z_4\right) \\ Tz_0^{\mathbf{i}} = \dfrac{D\mathbf{i}}{\mu^{(0)} h' k_T}\left(Ak_1^3 z_1 + Bk_2^3 z_2 + Uk_3^3 z_3 + Vk_4^3 z_4\right) \end{cases} \tag{5}$$

with $z_0 = e^{k_T \frac{L}{2}}$ and $z_i = e^{k_i \frac{L}{2}} (i = 1, 2, 3 \text{ and } 4)$. $\mu^{(0)}$ is the shear modulus of the base material. Solving Eq. (5) yields the transmission and reflection coefficients, yet the analytical solutions are not easy to be obtained. Towards this end, the above problem is re-formulated in another way, where the total wave fields are divided into two parts: the symmetric and anti-symmetric modes as done in Refs. 60

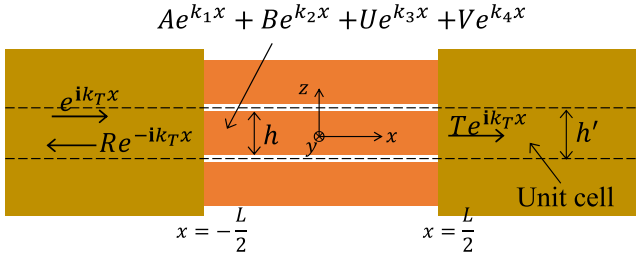

FIG. 2. The unit cell (between the two dash lines) used to analyze the transmission spectrum of this filter.

and 61. The wave fields for the symmetric and anti-symmetric modes are written respectively as:

$$w_S(x) = \begin{cases} e^{\mathbf{i}k_T x} + A_{1S} e^{-\mathbf{i}k_T x}, x < -\dfrac{L}{2} \\ C_{1S}\cos(|k_1|x) + D_{1S}\left(e^{k_3 x} + e^{-k_3 x}\right), |x| < \dfrac{L}{2} \\ e^{-\mathbf{i}k_T x} + A_{1S} e^{\mathbf{i}k_T x}, x > \dfrac{L}{2} \end{cases} \tag{6}$$

and

$$w_A(x) = \begin{cases} e^{\mathbf{i}k_T x} + A_{1A} e^{-\mathbf{i}k_T x}, x < -\dfrac{L}{2} \\ C_{1A}\sin(|k_1|x) + D_{1A}\left(e^{k_3 x} - e^{-k_3 x}\right), |x| < \dfrac{L}{2} \\ -e^{-\mathbf{i}k_T x} - A_{1A} e^{\mathbf{i}k_T x}, x > \dfrac{L}{2} \end{cases} \tag{7}$$

where A_{1S}, C_{1S}, D_{1S}, A_{1A}, C_{1A}, and D_{1A} are the unknown coefficients to be determined. It is easy to check that $w_S(-x) = w_S(x)$ and $w_A(-x) = -w_A(x)$. The total wave field, i.e., $w(x) = w_S(x) + w_A(x)$, has the following expression:

$$w(x) = \begin{cases} 2e^{\mathbf{i}k_T x} + (A_{1S} + A_{1A})\, e^{-\mathbf{i}k_T x}, x < -\dfrac{L}{2} \\ C_{1S}\cos(|k_1|x) + C_{1A}\sin(|k_1|x) + (D_{1S} + D_{1A})\, e^{k_3 x} + (D_{1S} - D_{1A})\, e^{-k_3 x}, |x| < \dfrac{L}{2} \\ (A_{1S} - A_{1A})\, e^{\mathbf{i}k_T x}, x > \dfrac{L}{2} \end{cases} \tag{8}$$

which is similar to that in Eq. (4). The symmetric and anti-symmetric modes are solved separately according to the same continuity conditions used in Eq. (5). As an illustration, the corresponding continuity conditions for the symmetric mode can be listed as:

$$\begin{cases} z_0^{-\mathbf{i}} + A_{1S} z_0^{\mathbf{i}} = C_{1S}\cos\left(|k_1|L/2\right) + D_{1S}\left(z_3^{-1} + z_3\right) \\ z_0^{-\mathbf{i}} - A_{1S} z_0^{\mathbf{i}} = -\mathbf{i}\tau\left[C_{1S}\sin\left(|k_1|L/2\right) + D_{1S}\eta\left(z_3^{-1} - z_3\right)\right] \\ z_0^{-\mathbf{i}} - A_{1S} z_0^{\mathbf{i}} = \dfrac{\mathbf{i}D|k_1|^3}{\mu^{(0)}h' k_T}\left[-C_{1S}\sin\left(|k_1|L/2\right) + D_{1S}\eta^3\left(z_3^{-1} - z_3\right)\right] \end{cases} \tag{9}$$

with $\tau = \frac{|k_1|}{k_T}$ and $\eta = \left|\frac{k_3}{k_1}\right|$. The analytical solution for A_{1S} is obtained as:

$$A_{1S} = \frac{\frac{1}{\eta(1+\eta^2)}\left(\frac{1}{t_h} + \frac{\eta}{t}\right)\left(1 - \frac{\mu^{(0)}h'}{D|k_1|^2}\right) - \left(\tau\mathbf{i} + \frac{1}{t}\right)}{\frac{1}{\eta\,(1+\eta^2)}\left(\frac{1}{t_h} + \frac{\eta}{t}\right)\left(1 - \frac{\mu^{(0)}h'}{D|k_1|^2}\right) + \left(\tau\mathbf{i} - \frac{1}{t}\right)} e^{-\mathbf{i}k_T L} \tag{10}$$

with $t = \tan\left(|k_1|\,\frac{L}{2}\right)$ and $t_h = \tanh\left(|k_3|\,\frac{L}{2}\right)$. The anti-symmetric mode can be solved similarly, leading to the analytical expression for A_{1A} as:

$$A_{1A} = \frac{\frac{1}{\eta\,(1+\eta^2)}\left(-t_h + \eta t\right)\left(1 - \frac{\mu^{(0)}h'}{D|k_1|^2}\right) + (\tau\mathbf{i} - t)}{\frac{1}{\eta\,(1+\eta^2)}\left(-t_h + \eta t\right)\left(1 - \frac{\mu^{(0)}h'}{D|k_1|^2}\right) - (\tau\mathbf{i} + t)} e^{-\mathbf{i}k_T L} \tag{11}$$

According to the wave fields expressed in Eq. (8), the transmission and reflection coefficients are calculated as:

$$\begin{cases} T = (A_{1S} - A_{1A})/2 \\ R = (A_{1S} + A_{1A})/2 \end{cases} \tag{12}$$

Results indicate that solutions from Eq. (5) are the same as those based on Eqs. (10–12).

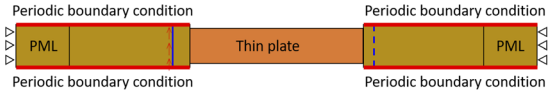

FIG. 3. The numerical model used in this paper.

IV. FEM NUMERICAL SIMULATIONS

To validate the feasibility of the designed filter, a series of numerical simulations using the FEM are conducted. Figure 3 plots the used numerical model, the rectangle in the middle represents the thin plate and the connected two parts are the base material. In the numerical simulations, the thin plate is perfectly bonded to the base blocks and the entire domain is discretized using plain-strain quadrilateral elements. The perfectly matched layers (PML) are employed at both ends to yield non-reflecting boundaries. In order to mimic the periodicity of the current design in the vertical direction, the periodic boundary conditions are applied on the top and bottom edges of the base blocks as the red lines shown. The horizontal displacement is fixed at the two exterior ends in order to avoid rigid motion. A uniform vertical displacement is applied on the left solid blue line to yield a plane SV wave (see red arrows). The vertical displacement at the right dashed blue line is obtained to calculate the transmission coefficient.

V. RESULTS AND DISCUSSIONS

A. Comparison between analytical results and numerical simulations

Figure 4 shows the transmission spectrum of this filter made up of thin PMMA plates when the base material is aluminum. The material properties of PMMA and aluminum are tabulated in Table I. The size of the thin PMMA plates is L=0.05m, h=0.005m, and h'=0.0055m. For a comparison, theoretical solutions from both the Kirchhoff and Mindlin plate theories have been plotted. The results show that all the transmission spectrums of this current filter from the two theories and numerical simulations have several sharp peaks, where the incident SV wave is transmitted through the filter without loss. However, t his is not the case for the transmission spectrum of the design with plates composed of the same material as the base material. At lower frequencies, both the two analytical solutions match well the numerical results, however, the solution based on Kirchhoff plate theory

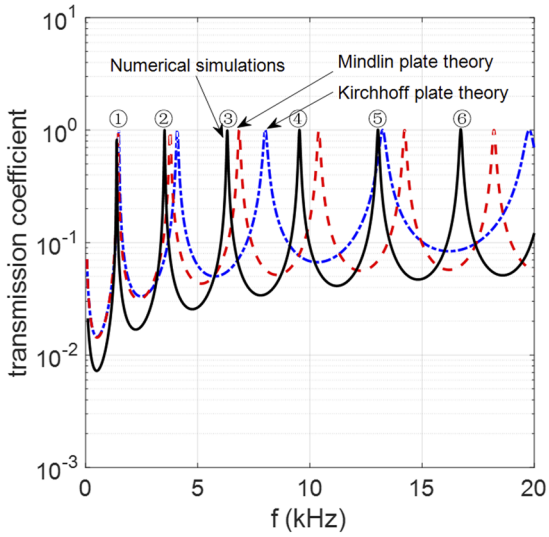

FIG. 4. The transmission spectrum of the designed filter obtained from the analytical models and the FEM numerical simulation.

TABLE I. The materials used in the present work.

	E(GPa)	υ	ρ(kg/m^3)
PMMA	0.53	0.37	1180
Aluminum	70.0	0.35	2700
Steel	210.0	0.29	7800
Copper	210.0	0.25	8500

deviates significantly from the numerical simulations at higher frequencies. The main reason is that, at high frequencies, the rotatory inertia and shear deformation effects become important.

The calculated vibration modes of the plate at the peaks are plotted in FIG. 5. The results show that the vibration direction of the transmitted wave is opposite to that of the incident wave at peaks ①, ③ and ⑤, while they are kept in pace at peaks ②, ④ and ⑥. This fact is also illustrated by the curve of real and imaginary parts of the transmission coefficient T as shown in FIG. 6. The peaks occur as the imaginary part of transmission coefficients equals zero and the absolute value of real parts equals one. At the corresponding peaks ①, ③ and ⑤, the real part of analytical transmission coefficients equals minus one, and is equal to positive one at the peaks ②, ④ and ⑥.

B. Other potential materials suitable to constitute the plates

In our previous paper, only the PMMA was considered to make the thin plates. In this work, other potential materials suitable for the thin plates are also discovered, which opens more opportunities. From FIG. 4, it is clear that the performance of this filter is determined by two factors: one is the existence of the peaks, and the other is the average value of the transmission coefficients over the investigated frequency range. As the peaks exist, a smaller mean value of the transmission coefficients indicates the filter has a better performance to inhibit other waves. Hence, the average transmission coefficients of filters with plates made of different materials are calculated using the theoretical model (Eqs. (10)–(12)) and illustrated in FIG. 7. For comparison, the result of PMMA denoted as the cross

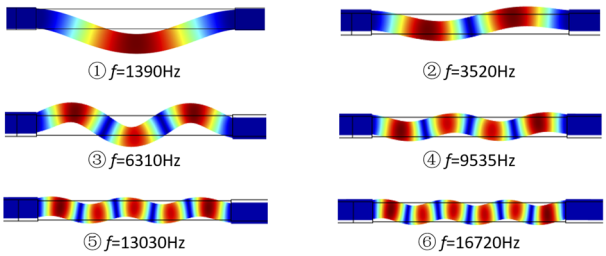

FIG. 5. Magnitude of the vertical displacement fields at the peaks of the numerical simulation results illustrated in FIG. 4.

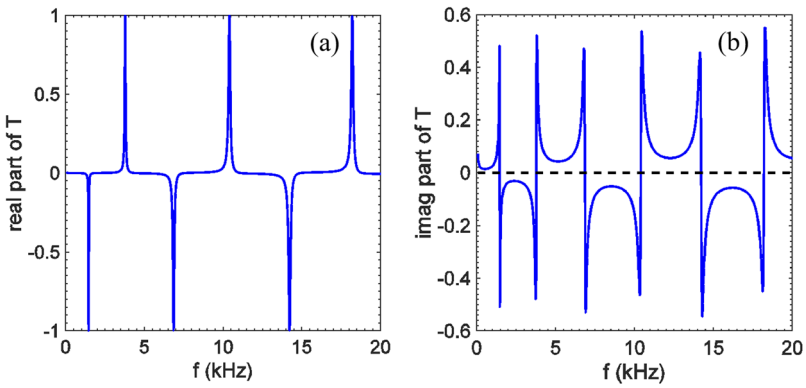

FIG. 6. Real (a) and imaginary (b) part of analytical (Mindlin plate theory) transmission coefficient *vs* frequencies.

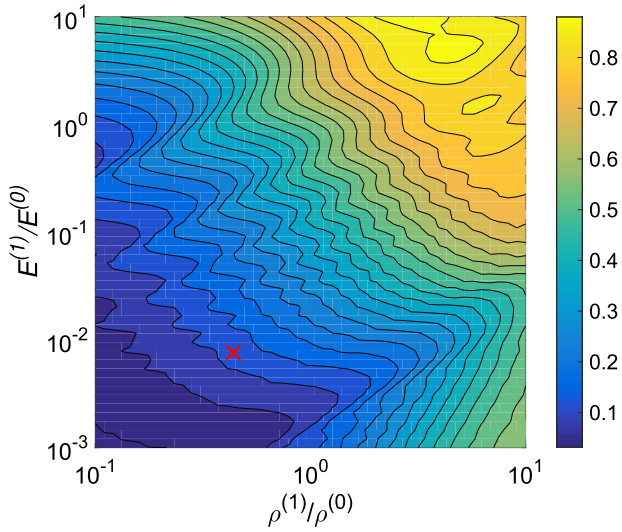

FIG. 7. The contour plot of average transmission coefficients of the current filter over 0 KHz~20 KHz versus material properties of the thin plates. The base material is aluminum and L=0.05m, h=0.005m, and h'=0.0055m. The Poisson's ratio of plates is assumed to be the same as that of the base material. $E^{(1)}/E^{(0)}$ is the ratio of Young's modulus between plates and the base material, and $\rho^{(1)}/\rho^{(0)}$ is the corresponding ratio of mass density.

dot is also plotted, the corresponding value for PMMA is 0.137. The results in this figure indicate that, in order to design a high-quality current filter, both the mass density and the Young's modulus of plates should be smaller than those of the base material.

C. The performance of this filter for waves in different base materials

Figure 8 shows the numerically calculated transmission coefficient of this filter for different base materials. It is clearly seen that the transmission spectrums of the current design show sharp peaks for all these three base materials. Moreover, the peaks occur at the same frequency points even the base material changes. This fact greatly benefits the development and application of the filters for elastic SV waves in various metals. The reason behind this fact can be referred to FIG. 5, in which the

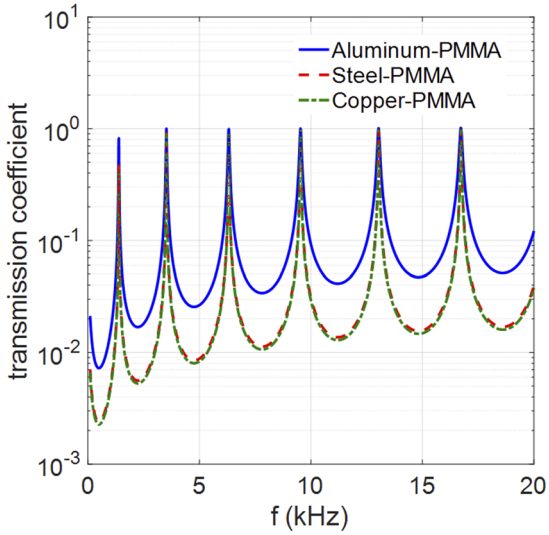

FIG. 8. The numerically calculated transmission spectrum of the designed filter under three different base materials. The geometry of the plate is: L=0.05m, h=0.005m, and h'=0.0055m. In the legend, the former represents the base material and the latter is the material of the plates.

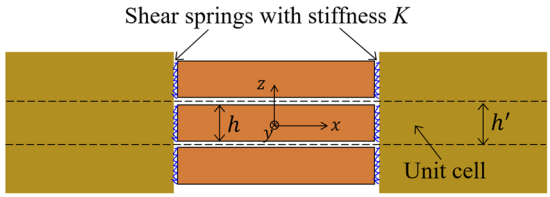

FIG. 9. The spring model used to investigate the bonding conditions of the interfaces on the performance of the current filter.

results show that the peaks happen at the natural frequencies of the plate of L with fixed displacement or opposite displacements at two ends.

D. The effect of bonding conditions of interfaces

In the above analysis and the previous work, the plates are assumed to be perfectly bonded to the base material at two ends. However, this is not true in practice. Here, the influence of the bonding condition between the plates and the base on the performance of this filter is analyzed using a spring model[62,63] as shown in FIG. 9, where the stresses and rotation angles are assumed to be continuous across the interfaces, while the displacements jump. Furthermore, the displacement jump is assumed to be linearly proportional to the stress at the interface. The ratio of the stress to the displacement jump is defined as the stiffness of the spring. Compared with Eq. (5), the corresponding equations taking the bonding condition into account are listed as follows,

$$\begin{cases} Az_1^{-1} + Bz_2^{-1} + Uz_3^{-1} + Vz_4^{-1} - \left(z_0^{-\mathbf{i}} + Rz_0^{\mathbf{i}}\right) = \dfrac{\mathbf{i}\mu^{(0)}h'k_T\left(z_0^{-\mathbf{i}} - Rz_0^{\mathbf{i}}\right)}{K} \\ z_0^{-\mathbf{i}} - Rz_0^{\mathbf{i}} = \dfrac{1}{\mathbf{i}k_T}\left(Ak_1z_1^{-1} + Bk_2z_2^{-1} + Uk_3z_3^{-1} + Vk_4z_4^{-1}\right) \\ z_0^{-\mathbf{i}} - Rz_0^{\mathbf{i}} = \dfrac{D\mathbf{i}}{\mu^{(0)}h'k_T}\left(Ak_1^3z_1^{-1} + Bk_2^3z_2^{-1} + Uk_3^3z_3^{-1} + Vk_4^3z_4^{-1}\right) \\ Tz_0^{\mathbf{i}} - (Az_1 + Bz_2 + Uz_3 + Vz_4) = \dfrac{\mathbf{i}\mu^{(0)}h'k_TTz_0^{\mathbf{i}}}{K} \\ Tz_0^{\mathbf{i}} = \dfrac{1}{\mathbf{i}k_T}(Ak_1z_1 + Bk_2z_2 + Uk_3z_3 + Vk_4z_4) \\ Tz_0^{\mathbf{i}} = \dfrac{D\mathbf{i}}{\mu^{(0)}h'k_T}\left(Ak_1^3z_1 + Bk_2^3z_2 + Uk_3^3z_3 + Vk_4^3z_4\right) \end{cases} \tag{13}$$

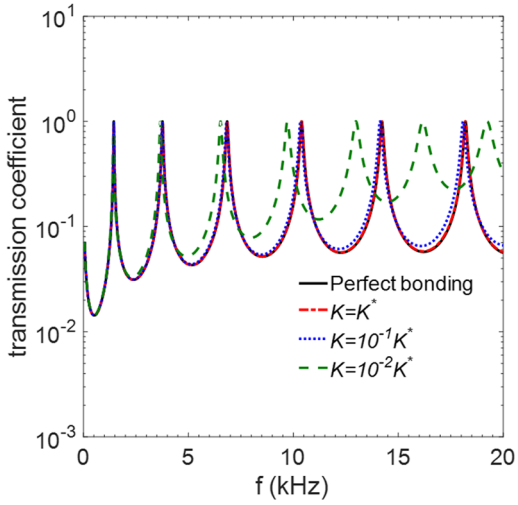

FIG. 10. Influence of the bonding condition of the interfaces between the base material and the plates on the transmission spectrum of the designed filter. The geometry of the plate is: L=0.05m, h=0.005m, and h'=0.0055m.

where K is the stiffness of the shear springs. Figure 10 shows the calculated transmission spectrum of the current filter for elastic SV waves in aluminum with the account of various bonding conditions at the two interfaces. The results show that the spring model with $K = 1.0K^*$ is close to the perfect bonding, where K^* equals $(E^{(0)} + E^{(1)})/2$. As the stiffness decreases, the peaks of the transmission spectrum generally shift from high frequencies to low frequencies, especially for those with a higher frequency. The effect of this imperfectly bonded interfaces on the peaks of low frequencies is almost negligible.

VI. CONCLUDING REMARKS

A narrow passband filter made with aligned parallel thin plates for the propagation of elastic SV waves in metals was designed. Based on the proposed unit cell, both the analytical model and the comprehensive numerical simulation verified the feasibility of the designed filter. For the analytical model, besides the classical Kirchhoff plate theory, the Mindlin plate theory with the account of rotatory inertia and shear deformation effects is also adopted to describe the dynamic behavior of the plates in the filter. Compared with the numerical simulations, the analytical model based upon the Mindlin plate theory gives more accurate results than the Kirchhoff plate theory. The calculated vibration modes indicate that the full transmission (peak) occur at the natural frequencies of the plate with fixed displacements or opposite displacements at the two ends. That is why the same filter works well for different base materials where the elastic SV waves propagate. The working frequencies of this filter can be easily adjusted by the change of geometries of the thin plates, specifically, the peaks shift from high frequencies to low frequencies as the length of the thin plates increases. The bonding condition of the interfaces between the thin plates and the base was also investigated using a spring model. Generally, the peaks shift from high frequencies to low frequencies as the bonding stiffness becomes weak. However, at low frequencies, the influence of this bonding stiffness becomes negligible. This filter has the potential to benefit the controlling of SV waves, such as mechanical vibration suppression, sensing, etc.

ACKNOWLEDGMENTS

This work was supported by the Chinese National Natural Science Fund (Grant 11502036 and 11632004) and the Natural Science Fund of the City of Chongqing (Grant cstc2015jcyjA0577). The Key Program for International Science and Technology Cooperation Projects of the Ministry of Science and Technology of China (No. 2016YFE0125900), the Guangxi Key Laboratory of Manufacturing Systems and Advanced Manufacturing Technology (No: 16-380-12-014k), and the Key Project of Natural Science Foundation of CQ CSTC (No. 0241002432002) also provided partial financial support. J Zhang thanks Xiaoshi Su from Rutgers University for the support on the numerical model and the technique of dividing the conventional transmission problem into the symmetric and anti-symmetric modes.

[1] Q. Wang, Y. Yang, X. Ni, Y.-L. Xu, X.-C. Sun, Z.-G. Chen, L. Feng, X.-p. Liu, M.-H. Lu, and Y.-F. Chen, Scientific Reports **5**, 10880 (2015).
[2] A. Khelif, P. A. Deymier, B. Djafari-Rouhani, J. O. Vasseur, and L. Dobrzynski, Journal of Applied Physics **94**, 1308 (2003).
[3] B. Liang, B. Yuan, and J. C. Cheng, Physical Review Letters **103**, 104301 (2009).
[4] M. I. Hussein, K. Hamza, G. M. Hulbert, and K. Saitou, Waves in Random and Complex Media **17**, 491 (2007).
[5] S. Halkjaer, O. Sigmund, and J. S. Jensen, Zeitschrift Fur Kristallographie **220**, 895 (2005).
[6] S. Hedayatrasa, K. Abhary, M. Uddin, and C.-T. Ng, Journal of the Mechanics and Physics of Solids **89**, 31 (2016).
[7] Y. M. Soliman, M. F. Su, Z. C. Leseman, C. M. Reinke, I. El-Kady, and R. H. Olsson III, Applied Physics Letters **97**, 193502 (2010).
[8] Z. Liu, X. Zhang, Y. Mao, Y. Y. Zhu, Z. Yang, C. T. Chan, and P. Sheng, Science **289**, 1734 (2000).
[9] X. Zhou, X. Liu, and G. Hu, Theoretical and Applied Mechanics Letters **2**, 041001 (2012).
[10] G. L. Huang and C. T. Sun, Journal of Vibration and Acoustics-Transactions of the ASME **132**, 031003 (2010).
[11] X. Wang, International Journal of Solids and Structures **51**, 1534 (2014).
[12] S. Yao, X. Zhou, and G. Hu, New Journal of Physics **10**, 043020 (2008).
[13] X. Y. An, H. L. Fan, and C. Z. Zhang, Journal of Sound and Vibration **409**, 217 (2017).
[14] X. An, F. Sun, P. Yu, H. Fan, S. He, and D. Fang, Journal of Applied Mechanics-Transactions of the ASME **82**, 031002 (2015).
[15] Y. Chen, G. Hu, and G. Huang, Journal of the Mechanics and Physics of Solids **105**, 179 (2017).
[16] P. F. Pai, H. Peng, and S. Jiang, International Journal of Mechanical Sciences **79**, 195 (2014).

[17] H.-H. Huang, C.-K. Lin, and K.-T. Tan, Smart Materials and Structures **25**, 085027 (2016).
[18] Y. Xiao, J. Wen, and X. Wen, Physics Letters A **376**, 1384 (2012).
[19] H. Khales, A. Hassein-Bey, and A. Khelif, Journal of Vibration and Acoustics-Transactions of the ASME **135**, 041007 (2013).
[20] S. Zuo, T. Ni, X. Wu, and J. Fan, Journal of Vibration and Control **23**, 1663 (2017).
[21] L. Ding, H.-P. Zhu, and T. Yin, Journal of Sound and Vibration **332**, 6377 (2013).
[22] M. Oudich, Y. Li, B. M. Assouar, and Z. Hou, New Journal of Physics **12**, 083049 (2010).
[23] K. Yu, T. Chen, and X. Wang, Physica B-Condensed Matter **416**, 12 (2013).
[24] T.-T. Wu, Z.-G. Huang, T.-C. Tsai, and T.-C. Wu, Applied Physics Letters **93**, 111902 (2008).
[25] J.-C. Hsu, Journal of Physics D-Applied Physics **44**, 055401 (2011).
[26] Y. Pennec, B. Djafari-Rouhani, H. Larabi, J. O. Vasseur, and A. C. Hladky-Hennion, Physical Review B **78**, 104105 (2008).
[27] M. B. Assouar and M. Oudich, Applied Physics Letters **100**, 123506 (2012).
[28] H.-J. Zhao, H.-W. Guo, B.-Y. Li, Z.-Q. Deng, and R.-Q. Liu, Journal of Applied Physics **118**, 044906 (2015).
[29] M. B. Assouar, J.-H. Sun, F.-S. Lin, and J.-C. Hsu, Ultrasonics **54**, 2159 (2014).
[30] A. Song, X. Wang, T. Chen, P. Jiang, and H. Bao, International Journal of Modern Physics B **30**, 1650029 (2016).
[31] T. Y. Huang, C. Shen, and Y. Jing, Journal of the Acoustical Society of America **139**, 3239 (2016).
[32] X. Wang, H. Zhao, X. Luo, and Z. Huang, Applied Physics Letters **108**, 041905 (2016).
[33] J. Mei, G. Ma, M. Yang, Z. Yang, W. Wen, and P. Sheng, Nature Communications **3**, 756 (2012).
[34] Z. Yang, J. Mei, M. Yang, N. H. Chan, and P. Sheng, Physical Review Letters **101**, 204301 (2008).
[35] Y. Chen, G. Huang, X. Zhou, G. Hu, and C.-T. Sun, Journal of the Acoustical Society of America **136**, 2926 (2014).
[36] Y. Chen, G. Huang, X. Zhou, G. Hu, and C.-T. Sun, Journal of the Acoustical Society of America **136**, 969 (2014).
[37] H.-W. Dong, Y.-S. Wang, and C. Zhang, Ultrasonics **76**, 109 (2017).
[38] X. N. Liu, G. K. Hu, C. T. Sun, and G. L. Huang, Journal of Sound and Vibration **330**, 2536 (2011).
[39] R. Zhu, X. N. Liu, G. K. Hu, C. T. Sun, and G. L. Huang, Nature Communications **5**, 5510 (2014).
[40] Y.-F. Wang, Y.-S. Wang, and C. Zhang, Journal of the Acoustical Society of America **139**, 3310 (2016).
[41] R. Zhu, Y. Y. Chen, M. V. Barnhart, G. K. Hu, C. T. Sun, and G. L. Huang, Applied Physics Letters **108**, 011905 (2016).
[42] Y. Y. Chen, G. K. Hu, and G. L. Huang, Smart Materials and Structures **25**, 105036 (2016).
[43] E. A. F. Parra, A. Bergamini, B. Van Damme, and P. Ermanni, Applied Physics Letters **110**, 184103 (2017).
[44] E. Bortot and G. Shmuel, Smart Materials and Structures **26**, 045028 (2017).
[45] T. Yang, Z.-G. Song, E. Clerkin, Y.-W. Zhang, J.-H. Sun, Y.-S. Su, L.-Q. Chen, and P. Hagedorn, AIP Advances **7**, 095323 (2017).
[46] A. Baz, New Journal of Physics **11**, 123010 (2009).
[47] Y. Y. Chen, G. L. Huang, and C. T. Sun, Journal of Vibration and Acoustics-Transactions of the ASME **136**, 061008 (2014).
[48] L. Airoldi and M. Ruzzene, New Journal of Physics **13**, 113010 (2011).
[49] F. Langfeldt, J. Riecken, W. Gleine, and O. von Estorff, Journal of Sound and Vibration **373**, 1 (2016).
[50] Y. Pennec, B. Djafari-Rouhani, J. O. Vasseur, A. Khelif, and P. A. Deymier, Physical Review E **69**, 046608 (2004).
[51] P. Zhang and A. C. To, Applied Physics Letters **102**, 121910 (2013).
[52] I. K. Lee, Y. J. Kim, J. H. Oh, and Y. Y. Kim, AIP Advances **3**, 3 (2013).
[53] I. K. Lee, H. M. Seung, and Y. Y. Kim, Journal of Sound and Vibration **355**, 86 (2015).
[54] Y. Pennec, B. Djafarirouhani, J. O. Vasseur, H. Larabi, A. Khelif, A. Choujaa, S. Benchabane, and V. Laude, Applied Physics Letters **87**, 141 (2005).
[55] R. P. Moiseyenko, Y. Pennec, R. Marchal, B. Bonello, and B. Djafari-Rouhani, Physical Review B **90**, 134307 (2014).
[56] Y. Pennec, B. D. Rouhani, H. Larabi, A. Akjouj, and G. Leveque, New Journal of Physics **14**, 073039 (2012).
[57] J. Zhang, Y. Liu, W. Yan, and N. Hu, AIP Advances **7**, 085318 (2017).
[58] X. Su, Z. Lu, and A. N. Norris, Journal of Applied Physics **123**, 091701 (2018).
[59] C. C. Mow and Y. H. Pao, *The diffraction of elastic waves and dynamic stress concentrations* (1971).
[60] X. S. Su and A. N. Norris, Journal of the Acoustical Society of America **139**, 3386 (2016).
[61] A. J. Nagy, Dissertations & Theses - Gradworks (2011).
[62] N. M. Newmark, Proceeding of the Society for Experimental Stress Analysis **9**, 75 (1951).
[63] S. I. Rokhlin, W. Huang, and Y. C. Chu, Ultrasonics **33**, 351 (1995).